



Contents lists available at ScienceDirect

Journal of Photochemistry & Photobiology, A: Chemistry

journal homepage: www.elsevier.com/locate/jphotochem

A boron-nitrogen heterocyclic AIE probe for sensitive detection of picric acid

Cheng Cheng^a, Miriam Roberto^a, Gianluca Destro^a, Rachele Stefania^b, Carla Carrera^c, Enzo Terreno^{a,*}^a Department of Molecular Biotechnology and Health Sciences, Molecular & Preclinical Imaging Centers, University of Torino, 10126 Torino, Italy^b Department of Science and Technological Innovation University of Eastern Piedmont "Amedeo Avogadro", 15120 Alessandria, Italy^c Institute of Biostructures and Bioimaging (IBB), Italian National Research Council (CNR), 10126 Torino, Italy

ARTICLE INFO

Keywords:

Aggregation-induced emission
 Detect picric acid
 Fluorescence sensor
 Paper sensor
 Quick detection

ABSTRACT

This article describes the design and synthesis of a B-N bond-based sensor (BNOH) to detect picric acid (PA), which is easy to synthesize with a high yield. It exhibits aggregation-induced emission (AIE) effect, and its solid bright fluorescence makes it suitable for use as a sensor. As PA sensor, BNOH performs excellently with good selectivity and sensitivity (detection limits as low as 2.9 ppb). The PA response mechanism of BNOH to PA was explored through computational simulation methods. Interestingly, trace amounts of solid PA can be detected by wiping the BNOH paper sensor, achieving convenient and quick PA detection.

1. Introduction

Picric acid (PA, 2,4,6-trinitrophenol) is an organic strong acid widely present in military, explosives, dyes, pesticides, leather, pharmaceuticals and chemical industries. It has a high destructive power, causing huge damage to human beings and environment. [1–5] The health hazards of picric acid mainly manifest as irritation to the skin and eyes. It can also cause damage to internal organs such as the immune system, liver and spleen. In extreme cases it may even lead to respiratory distress or other serious consequences. Due to its strong water solubility, once entering water bodies, it can contaminate groundwater and soil causing severe damage to farmland and natural environments.[6] Moreover, picric acid may be abused by terrorists posing a potential threat of terrorist attacks which brings security risks for society. The destructive power of picric acid is even stronger than TNT; slight friction on PA powder could trigger explosions.

To timely and accurately detect the presence of picric acid, various methods have emerged including Surface-Enhanced Raman Spectroscopy (SERS),[7,8] X-ray Diffraction (XRD),[9] Gas Chromatography-Mass Spectrometry (GC-MS), [10–12] Nuclear Quadrupole Resonance (NQR),[13–17] Ion Mobility Spectrometry (IMS)[18–22] and Cyclic Voltammetry. However, all these methods have certain limitations. SERS is a spectroscopic technique based on surface-enhanced effect that provides high sensitivity detection. However, the adsorption behavior of

PA might be affected by substrate materials or environmental conditions leading to signal changes or instability. In addition, the low concentration detection of PA might be influenced by background interference reducing accuracy. XRD is used for determining material structure and composition, but crystal structures are difficultly obtained during PA detection. GC-MS, is commonly used for analysis and identification of organic compounds. However, due to high sample pre-treatment requirements in PA detection, complex extraction and purification steps may be needed which is time-consuming and laborious. In electrochemical methods, PA might adsorb unstably on electrode surface leading to signal changes resulting in unreliable detection results.

Fluorescence detection technology has unique advantages in detecting explosives.[23–26] Using fluorescent probes such as emitting conjugated dendrimers,[27] poly silanes,[28], carbon quantum dots, [29–33]metal nanoclusters,[34–38]metal gels,[39,40]Metal-Organic Frameworks(MOF),[41–45]organic conjugated polymers,[46]organic small molecules,[47,48] and nano-composite materials, high-sensitive PA detection can be achieved. Compared with traditional detection methods, the fluorescence method has many advantages, including high detection sensitivity and fast response. The development of fluorescent probes with specific detection of PA can make it possible to combine PA with the probes under certain circumstances to produce spectral differentiation, thus enabling easy and fast identification of this harmful substance.[49]. Furthermore, the fluorescence method is non-

* Corresponding author.

E-mail address: enzo.terreno@unito.it (E. Terreno).<https://doi.org/10.1016/j.jphotochem.2024.115462>

Received 16 October 2023; Received in revised form 28 December 2023; Accepted 7 January 2024

Available online 13 January 2024

1010-6030/© 2024 The Author(s). Published by Elsevier B.V. This is an open access article under the CC BY license (<http://creativecommons.org/licenses/by/4.0/>).

destructive and pollution-free, thus avoiding additional harm or contamination to the object being tested. Therefore, the fluorescence method has broad application prospects in the field of picric acid detection providing a feasible modern strategy for protecting human health and environmental safety.

Aggregation-induced emission (AIE) is an emerging fluorescent phenomenon first proposed by Benzhong Tang's research team in 2001. [50] AIE refers to the phenomenon where a fluorophore exhibits a significant increase in fluorescence emission upon transitioning from a monomeric state to an aggregated state. Compared with traditional fluorescent probes, AIE has a series of obvious advantages. The strong fluorescence emission induced by AIE allows for achieving excellent sensitivity and enabling rapid detection at low concentration targets. [51–54] Due to its aggregate-emission feature, AIE easily overcomes the problem where traditional fluorescent probes are quenched due to agglomeration when placed into water. Furthermore, it does not require complex synthesis methods for improving molecular water solubility, thus enabling sensitive detection of the target in water. AIE molecules also show excellent photostability, able to withstand long-term light exposure without fluorescence attenuation, maintaining persistent signal output. Therefore, AIE technology has been widely favored in multiple fields. In biomedical field, AIE molecules can be used for cell imaging, tumor diagnosis and drug delivery, realizing real-time monitoring of biological processes through specific interactions with biological tissues. [55,56] In environmental field, AIE molecules can be used for water quality monitoring, pollutant detection and food safety, [57] keeping advantages such as rapid response, high sensitivity and selectivity. On this basis, the development of an AIE probe for PA detection may have a great significance and broad prospects.

Here, we have designed and reported a novel B-N bond-based AIE probe, BNOH, for a rapid, sensitive, and accurate detection of PA. BNOH is synthesized easily in one step with excellent purity and yield. The properties of BNOH were studied in detail by spectroscopy to explore the interaction between BNOH and PA. In addition, we optimized the molecular model using density functional theory (DFT) to explain the possibility of fluorescence quenching during the detection process. Finally, we prepared paper sensors using BNOH solution for portable detection. The paper sensor has excellent detection efficiency and limit with simple usage, just contact with powder under UV light, to observe results.

2. Experiment

2.1. Materials and methods

Unless otherwise noted, materials (including a 10 µg/L PA solution in acetonitrile) were purchased from Sigma and used without further purification. For a series of organic molecules, potentially interfering with PA detection, such as benzoic acid, p-nitrophenol, nitrobenzene, and phenol, 10 mL of 1 M stock solutions in THF were prepared. Dichloromethane was distilled from CaH. Toluene was purified by refluxing sodium in nitrogen for several hours and then distilled to remove trace of water. Deionized water was obtained by Milli-Q purification system (Millipore) with electrical conductivity of 18.2 s/m. Using tetramethylsilane (TMS) as the internal standard, ¹H and ¹³C NMR spectra were recorded on a 14 T Bruker Avance III spectrometer. Mass spectra were recorded on the Brook Electron spray Ionization Mass Spectrometer (ESI-MS). The UV–Vis absorption spectra were obtained on CARY50 biological spectrophotometer (Varian Inc., CA., USA). Fluorescence spectra were obtained on a Fluoromax-4 spectrofluorimeter (Horiba Jobin Yvon Inc., USA).

2.2. Synthesis of BNOH

Naphthalene-1,8-diamine (158 mg, 1 mmol) and (4-hydroxyphenyl) boronic acid (150 mg, 1.08 mmol) were dissolved in anhydrous toluene

and refluxed for 10 h under argon protection. The product was obtained by removing the solvent through rotary evaporator. Purification was achieved by extraction with deionized water and ethyl acetate (25 mL, four times), separating the organic phase, drying it with sodium sulphate, filtering it, and then subjecting the filtrate to pressure distillation. The product was purified by silica gel column chromatography using Dichloromethane as eluent. The resulting product (white solid, 220 mg) was obtained with a yield of 84.6 %. ¹H NMR (600 MHz, MeOD) δ 7.70 (d, *J* = 7.9 Hz, 2H), 7.50 (s, 2H), 7.07 (t, *J* = 7.8 Hz, 2H), 6.92 (d, *J* = 8.1 Hz, 2H), 6.85 (d, *J* = 7.8 Hz, 2H), 6.52 (d, *J* = 7.3 Hz, 2H). ¹³C NMR (151 MHz, MeOD) δ 159.00, 142.60, 136.59, 133.60, 127.23, 119.90, 116.25, 114.59, 104.74. MS (ESI) *m/z* for C₁₆H₁₂BN₂O calculated 260.11 [M + H⁺] found: 261.21. These observations fully agree with literature data. [54].

2.3. Formation of BNOH aggregates

2.6 mg of solid BNOH were dissolved in 1 mL of methanol to obtain a 10 mM BNOH solution, which was stored in the dark at 4 °C. At room temperature, 100 µL of the BNOH methanol solution were dropwise added into 48 mL of 1 mM PBS buffer (pH = 6.8) and 1.9 mL MeOH (96 % PBS/MeOH), stirred overnight to obtain a homogeneous solution containing the aggregated BNOH with a concentration of 20 µM. Unless otherwise specified, this solution was used for characterizing the UV–VIS, fluorescence properties and the PA detection of BNOH. [58] The response experiment with PA was conducted using the above-described solution of aggregated BNOH. The excitation wavelength for BNOH was set to 330 nm (3 nm of slit width).

2.4. Spectrofluorimetry of BNOH

The fluorescence properties of BNOH (final concentration 20 µM) were tested in solvents with different polarities: Dimethylformamide, Acetonitrile, Methanol, Tetrahydrofuran, Chloroform and n-Hexane.

2.5. Testing BNOH-PA interaction

Job's plot was used to characterize the interaction between PA and the BNOH sensor. In this experiment, a series of solutions obtained by mixing different volumes of the aggregated BNOH solution and PA to a fixed volume of 1 mL were prepared. The fluorescence spectra of the resulting solutions were acquired at room temperature.

$$F_{\text{job}} = (1-x) F_0 - F$$

x is the molar fraction of PA, *F*₀ and *F* are the fluorescence intensity of solution in the absence and presence of PA. The total molar concentration of the two components should be kept at a fixed value while the molar fraction of any component is variable. In this experiment, the total concentration of BNOH and PA was 4 × 10⁻⁵ M, and the molar fraction of PA in the mixture was 0, 0.1, 0.2, 0.3, 0.4, 0.5, 0.6, 0.7, 0.8, 0.9, and 1.0.

2.6. Limit of detection (LOD) experiments

The PA detection limit (3σ/*k*) of the BNOH sensor was calculated by analyzing the fluorescence of BNOH at different concentrations of PA. In the detection limit equation, σ is the standard deviation, and *k* is the slope of the linear curve. The standard deviation (σ) was obtained from the bank test of the aggregated BNOH solution in the absence of PA. The slope (*k*) was obtained by plotting the concentration of PA versus the fluorescence intensity.

2.7. Computational methods

DFT calculations (ORCA 5.0.31) [59] were used to optimize the

structure of the adduct formed between PA and BNOH in the non-aggregated monomeric form. Geometry optimization and frequency calculation were performed at the B3LYP-D3BJ/6-31G(D) theoretical level. To calculate interactions and eliminate the influence of Basis Set Superposition Error (BSSE), gCP correction was used in the calculation [60]. Molecular orbitals and electrostatic potential maps were obtained at the B3LYP-D3BJ/def2-TZPP level. BNOH and PA monomer molecules are optimized on gaussian09, and the results of molecular orbitals and electrostatic potential diagrams were obtained at B3LYP /6-31G(D) level.

2.8. Fabrication of a paper-based prototype of BNOH as PA sensor

A solution of 100 μM of BNOH in methanol was prepared. Filter paper was cut into appropriate sizes and immersed in the solution for 2 h. The paper was then taken out, laid flat on a glass plate, and air-dried in a fume hood before use.

3. Results and discussion

The synthetic route followed for obtaining BNOH is reported in Scheme 1. The compound was easily obtained by refluxing 2-aminonaphthalene with hydroxyphenylboronic acid in toluene. The Compound BNOH was characterized by ^1H NMR, ^{13}C NMR and Mass Spectrometry in (Fig. S1-3, Supporting Information). Although the structure of BNOH has been already reported in literature, [61–63] these reports only improved the synthesis method of BNOH but did not effectively apply it to detect explosive PA systems. In the structure of BNOH there are two electron-rich functional groups, the B-N bond region and hydroxyl group, which may effectively interact with PA. Both chemical entities are likely to produce photoinduced electron transfer effects during light excitation resulting in different emission characteristics. Therefore, we determined the photo physical properties of BNOH and its capability to act as PA sensor using UV and fluorescence spectroscopies as well as DFT calculations.

Firstly, we tested the basic spectral properties of BNOH. In MeOH, BNOH exhibited a broad UV absorption at 330 nm (Fig. 1A). The fluorescence emission showed two peaks at 381 nm and 425 nm (Fig. 1B), which originate from the vibration of phenol and naphthylamine moieties, respectively. This emissive pattern is confirmed in the spectra acquired in different solvents (Fig. 1C), with a slight red shift with the increase of solvent polarity. Table S1 reports the Stokes shift values of BNOH in different solvents. Although DMF is also a highly polar solvent, BNOH dissolves well in it, so its emission intensity is stronger than that in other solvents.

We also tested the fluorescence emission intensity (at 425 nm) of BNOH in methanol solution at different concentrations (Fig. S4). Within 100 μM concentration range, the fluorescence intensity progressively increased with concentration; however, when the concentration reached 500 μM , fluorescence started to be quenched and at 1 mM the system was not fluorescent anymore. From this observation, to ensure a good

detection sensitivity, a BNOH concentration of 20 μM for selected for the successive experiments.

Next, we investigated the photoluminescence properties of BNOH in water (Fig. 2A). By varying the water/methanol ratio, we found that as the water content increased, the emission spectrum of BNOH gradually changed the pattern and evolved to a single emission peak (centered at 400 nm) in the solution with the maximum water fraction (96 %), indicating aggregation of BNOH in water. The plot reporting the emission intensity at 425 nm (Fig. 2B), showed that when the proportion of water reached 70 %, the emission intensity of BNOH switched from quenching to AIE effect. This suggests that at a ratio of 70 %, BNOH started to aggregate. The UV spectra of BNOH are also displayed in Figure S5. From a ratio of 70 % onwards, the fluorescence keeps increasing due to the gradual insolubility of BNOH in the mixed MeOH/water solution, which is exhibiting a typical AIE phenomenon due to the formation of aggregates, as confirmed by the dynamic light scattering (DLS) results. (Fig. S6) The BN bond will behave like a carbon-carbon double bond in the structure, [58,64] as the aggregation proceeds, the vibration of the naphthalene ring connected by the B-N bond is suppressed, and the rotation of the benzene ring connected to the boron atom is also suppressed, and this part of the energy is used for light emission, resulting in AIE. Such behavior provides the rationale for using BNOH as fluorescent sensor in aqueous environments.

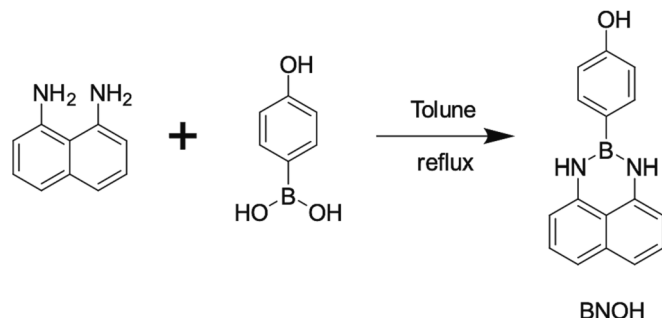
According to this hypothesis, we evaluated the ability of BNOH to detect picric acid. By adding different concentrations of PA (0–100 $\mu\text{g}/\text{mL}$ range) to a solution containing 20 μM BNOH (Fig. 3A), we found that as the concentration of PA increased, the fluorescence of BNOH was quenched and the final fluorescence intensity differed by a factor of 526 compared to the starting solution with no PA added. The quenching efficiency $[(I_0-I)/I_0]$ at 100 $\mu\text{g}/\text{mL}$ was 98.1 %. The quenching was linear with the PA concentration only in the 0–10 $\mu\text{g}/\text{mL}$ range (Fig. 3B), where the probe was very sensitive to the analyte (R-Square 0.98), resulting in a limit-of-detection (LOD) as low as 2.9 ppb. Fig. 3A indicates that upon increasing the PA concentration, the fluorescence experienced a red shift, which can be attributed to a photoinduced electron transfer (PET) between PA and BNOH. To delve deeper into the quenching dynamics, we computed the Stern – Volmer constant, revealing a value of $5.88 \times 10^8 \text{M}^{-1}$. To probe deeper into the sensitivity of PA detection using BNOH, Stern-Volmer plots were generated. As depicted in Fig. S7, at higher PA concentrations, the curve exhibited an upward bend, suggesting an over-amplified burst effect. [49] In contrast, at lower PA concentrations (0–20 $\mu\text{g}/\text{mL}$), the Stern-Volmer plot displayed linearity. The Stern – Volmer equation takes the form:

$$I/I_0 = 1 + K_{SV}[Q]$$

Here, I_0 represents the initial fluorescence intensity, while I signifies the final intensity subsequent to the introduction of the analyte, and $[Q]$ denotes the concentration of the analyte. [49].

To understand the binding mode and assess the stoichiometry of the interaction between BNOH and PA, we measured the fluorescence intensity at 425 nm of 1 mL solutions containing a different molar fraction of PA (x_{PA}) and BNOH (Job plot, Fig. S8). The result obtained is a clear indication that the maximum change in intensity occurs when x_{PA} is 0.46, indicating that a 1:1 complex is formed between the two interacting partners. However, even when more PA (1 to 2 equivalents) is added, the quenching is still observed. [65,66] Mass spectrometric analysis revealed distinctive changes when PA was introduced in varying quantities. Upon adding 0.2 equivalents of PA, a notable reduction in the molecular peak of BNOH at 260 was observed, accompanied by the emergence of a unique new peak at 429. Subsequent gradual addition of PA up to 0.6 equivalents resulted in the formation of a complex peak at 484. Further addition of PA to reach 1 equivalent led to the complete disappearance of peak 429, leaving behind only the newly emerged peak at 485. (Fig. S9).

We attempted to explain this phenomenon by optimizing the



Scheme 1. Synthesis route of BNOH.

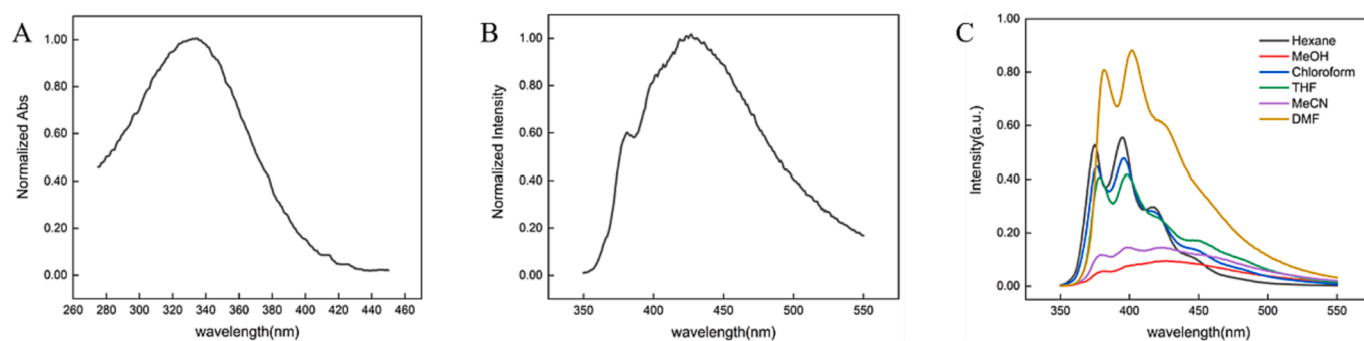


Fig. 1. (A) UV-Vis spectra of BNOH in MeOH. (B) fluorescence spectra of BNOH in MeOH. (C) Emission spectra of BNOH in different solvents.

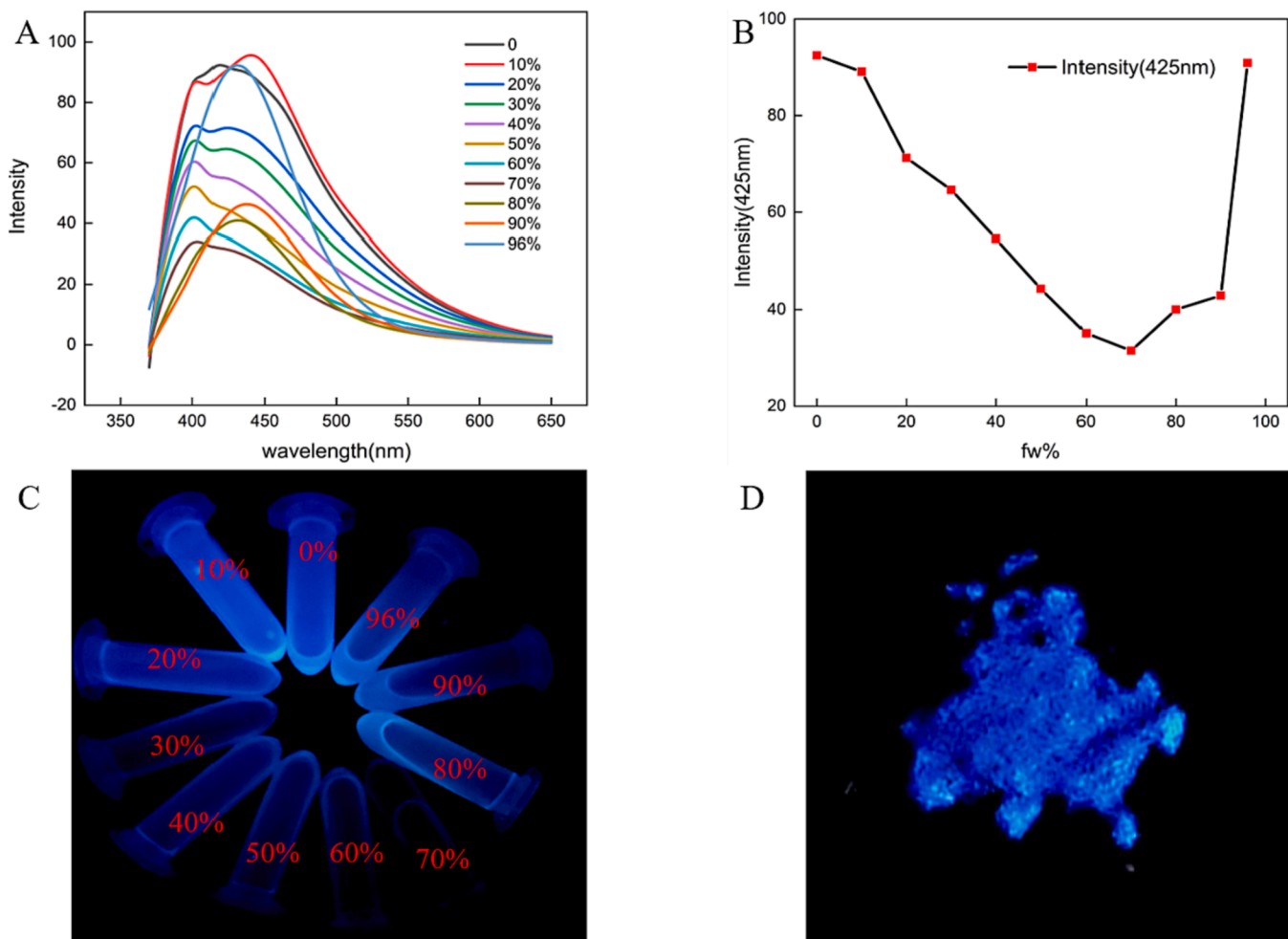


Fig. 2. (A) Emission spectra of BNOH in mixed solutions of water/methanol at different ratios. (B) Fluorescence intensity change curve of BNOH at 425 nm. (C) Optical color change of BNOH in different water/methanol percentage mixed solutions. (D) The luminescence of BNOH solid powder under ultraviolet lamp.

molecular model using density functional theory (DFT). The molecular structures of BNOH and PA were optimized using DFT (B3LYP/6-31G(D)) method, while the molecular structure of the BNOH/PA adduct was calculated using B3LYP-D3BJ/6-31G(D) method to ensure the comprehension of the quenching process. The results showed that PA and BNOH formed a planar arrangement (Fig. S10), which facilitates the recognition of PA by BNOH. During this process, BNOH forms π - π stacking with PA, and the NH hydrogens connected with boron can reinforce the interaction through hydrogen bonds with PA. Molecular orbital energy level calculation (Fig. 4) also showed different electronic arrangements. In the single molecules, the orbital distribution of BNOH was clear, with

HOMO located in naphthalene part and LUMO almost distributed throughout the molecule, with an energy difference of 4.08 eV. The orbital distribution of PA was simpler, with an energy difference around 4 eV. It is worth noting that the HOMO energy of PA is much lower than that of BNOH, so it is relatively more stable than BNOH. The LUMO energy of PA is between HOMO and LUMO energies of BNOH, only differing from HOMO by 0.69 eV; such low gap can easily promote the transfer of their joint excitation energy onto PA, thus resulting in fluorescence quenching feedback phenomenon.

The results obtained from the joint-optimization of both molecules are close to our guesswork: HOMOs orbitals still arrange at

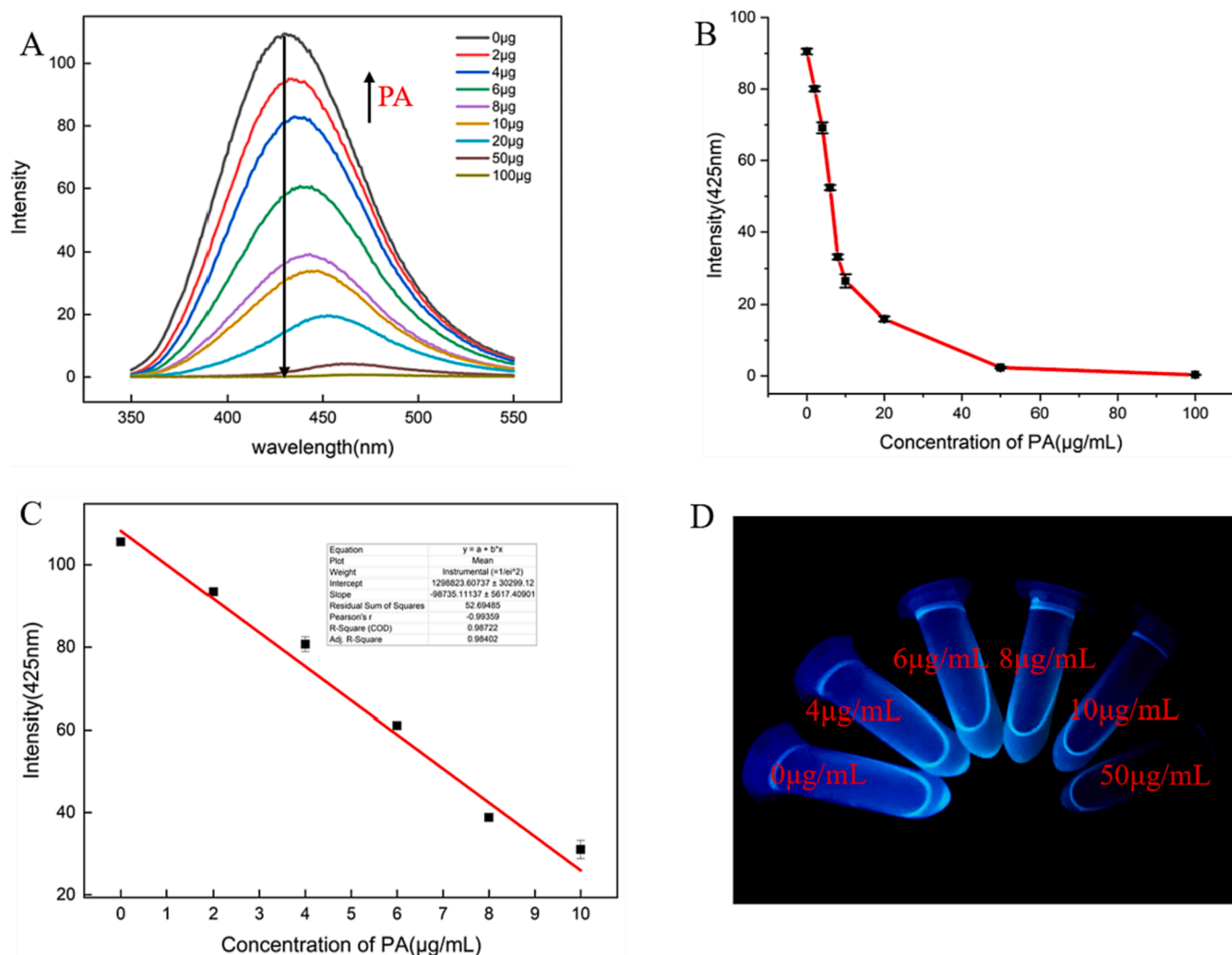


Fig. 3. (A) Fluorescence spectra of BNOH solution with different concentrations of PA. (B) Changes in fluorescence intensity of BNOH at 425 nm, (C) the linear relationship between fluorescence intensity at 425 nm and PA concentration, (D) The optical color of BNOH solution changes after adding different concentrations of PA.

naphthylamine moiety in composite molecule without significant change compared to individual ones; however, its total potential energy is reduced due to the influence of PA, which is -5.4 eV. The introduction of the PA molecule in the composite system has a significant impact on the LUMO orbital distribution of the BNOH monomer molecule, which is now predominantly distributed on the PA molecule. Additionally, the LUMO energy values of the complex molecules closely resemble that one of PA, with values of -3.68 eV and -3.93 eV, respectively. This represents a remarkable change compared to the BNOH monomer. Furthermore, the energy difference (ΔE) between the excited state and the ground state in the complex is significantly reduced from 4.08 eV to 1.72 eV. This reduction indicates that, upon excitation, BNOH absorbs energy and the electrons that would typically transition to the S1 orbital of BNOH now transition to the S1 orbital of PA. Subsequently, these electrons return to the ground state, resulting in a photoinduced electron transfer process. As a consequence of this transfer, the fluorescence of BNOH is effectively quenched.

The molecular electrostatic potential map (ESP) of BNOH and PA, as well as their complex, were calculated (Fig. S11). Blue and red represent the positive and negative potentials, respectively. The ESP maps obtained for BNOH and PA suggest that the drive-force of the formation of the adduct is the occurrence of non-covalent bonds with interaction energy calculated at -5.14 kcal/mol, supported by low-energy

interactions.

We believe that one the key factors in the formation of the adduct is the nitro functional group of PA, because the electron-deficient feature of this group can favor PET effects. To confirm the role of the nitro group, the fluorescence intensity of BNOH was measured in presence of different aromatic compounds (Figs. S12-S13). We found that the presence of a single nitro group (NB), as well as a single carboxylic group (BA), or a single hydroxyl group (PH) did not quench the fluorescence. Quenching was effective in presence of both one nitro and one hydroxyl groups (NP), though the quenching effect was much lower than PA, suggesting the role of the number of the two substituents. This observation is relevant to highlight the excellent selectivity of BNOH to act as PA sensor.

We also conducted some stability tests on BNOH. First, we assessed the stability of BNOH in water solution at different pH values (Figs. S14-S15). Due to the presence of phenolic group, whose pKa value is usually between 10 and 12, [67] BNOH is deprotonated in an alkaline environment and its electron conjugation structure is destroyed, resulting in fluorescence disappearance. Subsequently, we tested the photostability of BNOH (Fig. S16). Under continuous UV irradiation at 330 nm for 2 h, there was almost no change in UV absorption intensity, while a slight decrease was observed in the fluorescent emission intensity at 425 nm, which demonstrated an excellent photostability.

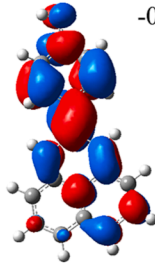
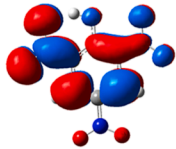
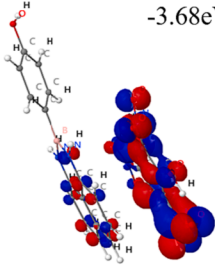

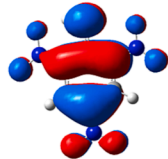
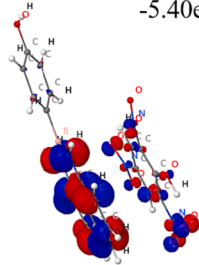
	BNOH	PA	PA+BNOH
LUMO	 -0.54eV	 -3.93eV	 -3.68eV
HOMO	 -4.62eV	 -8.30eV	 -5.40eV
ΔE	4.08eV	4.37eV	1.72eV

Fig. 4. Molecular orbital energy level distribution of BNOH, PA and their complex.

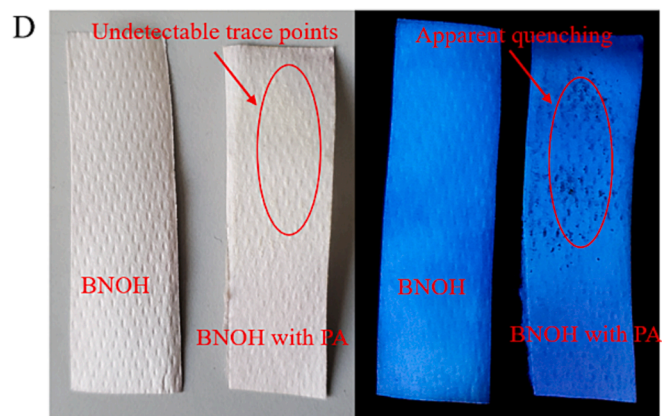
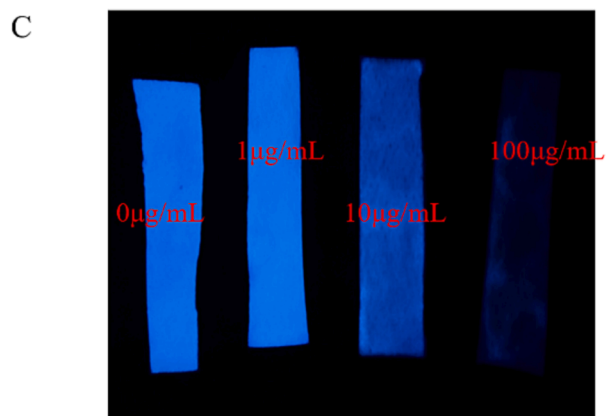
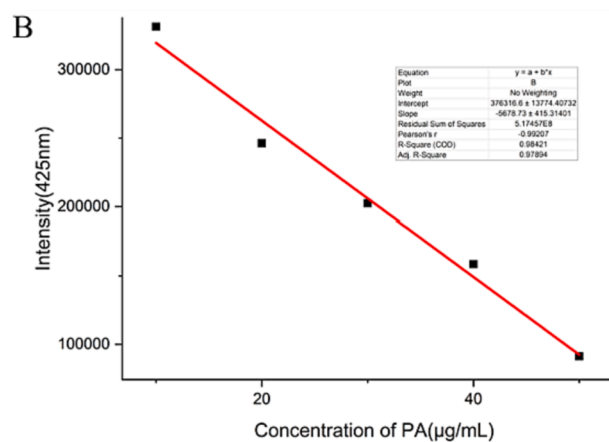
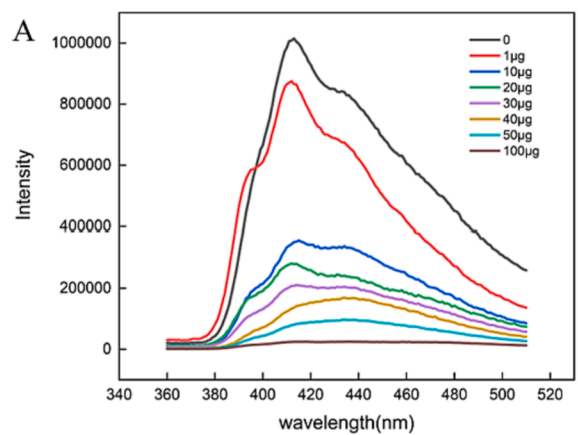


Fig. 5. (A) Emission of BNOH paper strips to detect PA in different concentrations. (B) Linearity of fluorescence intensity at 425 nm with PA concentration (10–50 µg/mL) for BNOH paper sensor. (C) Photo of BNOH paper strips to detect PA in different concentrations solution of PA under UV irradiation. (D) and solid PA under sunlight (left) or UV irradiation (right).

On this basis, BNOH appears to be a promising system to act as PA sensor. Currently, the detection of PA and, in general, explosives requires complex, costly, and time-consuming operations. Explosives can pose significant hazards when they come into contact with human skin or certain materials; even slight friction can cause explosions that may also contaminate water sources. Therefore, the development of rapid and convenient detection methods has a great significance.

To move a bit forward in this direction, we have developed a paper-based PA sensor based on BNOH by immersing paper strips for 2 h into a methanol solution containing 100 μM of BNOH, followed by drying the strips in a cool place. Then, we dipped the paper strip into acetonitrile solution containing PA or touched the strips with powdered PA to observe changes in the paper under UV light conditions (Fig. 5C). The fluorescence spectrum of BNOH-coated paper strips for detecting PA under 330 nm excitation was observed. Fig. 5A illustrates that with escalating PA concentrations, the fluorescence emission of the paper sensor diminishes consistently, exhibiting a linear correlation within the 10–50 $\mu\text{g}/\text{mL}$ range of PA concentrations (Fig. 5B), where the part of the paper that was in contact with PA reduced the fluorescence significantly, forming a clear contrast with the unreacted part. Since explosives often leave traces on clothing and bags, we also tested the performance of the strip-based sensor on trace amounts of solid PA. (Fig. 5D) We dropped different concentrations of PA solution onto a glass plate and dried it in a fume hood before wiping it with the paper-based sensor and observing under UV light. A quenched spot was clearly observed in the area of the strip that reacted with PA, highlighting the potential of this approach in detecting traces of solid PA.

4. Conclusion

In summary, we have synthesized and tested a fluorescent probe (BNOH) containing B-N bond and hydroxyl group for sensing the explosive picric acid. In aqueous environments, the probe produces a bright fluorescence caused by the AIE effect. The interaction between the BNOH aggregates and PA significantly quenches the emission with a high selectivity and sensitivity. The quenching results from the formation of a 1:1 adduct between BNOH and PA, stabilized by π - π stacking and generates photoinduced charge transfer upon light excitation, as demonstrated by DFT calculation. To preliminarily demonstrate the potential of this probe “on-field”, solid paper strips were pre-treated with BNOH and exposed to light after contact with the analyte, demonstrating an excellent sensitivity to detect PA both in solution and as powder. The results herein presented highlight the great potential of this probe for electronic sensing in real explosives, water pollutants, soil sensors, etc., playing a positive role in homeland security and explosive detection.

CRedit authorship contribution statement

Cheng Cheng: Writing – review & editing, Writing – original draft, Validation, Supervision, Methodology, Investigation, Formal analysis, Data curation, Conceptualization. **Miriam Roberto:** Investigation. **Gianluca Destro:** Data curation. **Rachele Stefania:** Methodology. **Carla Carrera:** Resources. **Enzo Terreno:** Writing – review & editing.

Declaration of competing interest

The authors declare that they have no known competing financial interests or personal relationships that could have appeared to influence the work reported in this paper.

Data availability

No data was used for the research described in the article.

Acknowledgements

We gratefully acknowledge the support of the FOE contribution of the Italian Ministry of Research to the Euro-BioImaging MultiModal Molecular Imaging Italian Node (www.mmmi.unito.it).

Appendix A. Supplementary data

Supplementary data to this article can be found online at <https://doi.org/10.1016/j.jphotochem.2024.115462>.

References

- [1] D.K. Wang, M. Wang, K.X. Chen, Y.J. You, J. Zhang, X.H. Zhou, W. Huang, A dual functional 1D Cd-based coordination polymer for the highly luminescent sensitive detection of Fe^{3+} and picric acid, *Appl. Organomet. Chem.* 34 (8) (2020).
- [2] M. Fabin, M. Lapkowski, T. Jarosz, Methods for Detecting picric acid—a review of recent progress, *Appl. Sci.-Basel* 13 (6) (2023).
- [3] P.F. Fan, C. Liu, Q.J. Li, C.C. Hu, X.W. Wu, X.H. Zhang, H. Liang, S.Y. Yang, Microwave-assisted rapid synthesis of ovalbumin-stabilized gold nanoclusters for picric acid determination, *J. Cent. South Univ.* 30 (1) (2023) 74–84.
- [4] A. Abbasi, M. Shakir, Simple One-step Solid-state Synthesis of Highly Crystalline N Doped Carbon Dots As Selective Turn Off-sensor for Picric Acid and Metanil Yellow, *J. Fluoresc.* 32 (3) (2022) 1239–1246.
- [5] T. Santiwat, N. Sornkaew, K. Srikitiwanna, N. Sukwattanasinitt, N. Niammont, Electrospun nanofiber sheets mixed with a novel triphenylamine-pyrenyl salicylic acid fluorophore for the selective detection of picric acid, *J. Photochem. Photobiol. A-Chem.* 434 (2023).
- [6] R.M. Farsi, N.M. Alharbi, F.S. Basingab, N.M. Nass, S.Y. Qattan, S.A. Hassoubah, J. S. Alrahimi, B.A. Alaidaroos, Biodegradation of picric acid (2,4,6-trinitrophenol, TNP) by free and immobilized marine *Enterococcus thallicaudus* isolated from the red sea, Saudi Arabia, *Egypt. J. Aquat. Res.* 47 (3) (2021) 307–312.
- [7] R. Beeram, V.S. Vendamani, V.R. Soma, Deep learning approach to overcome signal fluctuations in SERS for efficient On-Site trace explosives detection, *Spectrochim. Acta Part a-Mol. Biomol. Spectrosc.* 289 (2023).
- [8] D.Y. Lin, R.L. Dong, P. Li, S.F. Li, M.H. Ge, Y.F. Zhang, L.B. Yang, W.P. Xu, A novel SERS selective detection sensor for trace trinitrotoluene based on meisenheimer complex of monoethanolamine molecule, *Talanta* 218 (2020).
- [9] R.W. Madden, J. Mahdavi, R.C. Smith, R. Subramanian, An explosives detection system for airline security using coherent x-ray scattering technology., Conference on Hard X-Ray, Gamma-Ray, and Neutron Detector Physics X, San Diego, CA, 2008.
- [10] F.F. Tian, J. Yu, J.L. Hu, Y. Zhang, M.X. Xie, Y. Liu, X.F. Wang, H.L. Liu, J. Han, Determination of emulsion explosives with Span-80 as emulsifier by gas chromatography-mass spectrometry, *J. Chromatogr. A* 1218 (22) (2011) 3521–3528.
- [11] M.A.C. Hartel, T.M. Klapotke, J. Stierstorfer, L. Zehetner, Vapor pressure of linear nitrate esters determined by transpiration method in combination with VO-GC/MS, *Propellants Explos. Pyrotech.* 44 (4) (2019) 484–492.
- [12] T.H. Bunning, J.S. Strehse, A.C. Hollmann, T. Botticher, E. Maser, A Toolbox for the determination of nitroaromatic explosives in marine water, sediment, and biota samples on femtogram levels by GC-MS/MS, *Toxics* 9 (3) (2021).
- [13] M.C. Monti, D.A. Alexson, J.K. Okamitsu, NQR detection of explosive simulants using RF atomic magnetometers. Conference on Detection and Sensing of Mines, Explosive Objects, and Obscured Targets XXI, Baltimore, MD, 2016.
- [14] T. Nichols, S. Gidcumb, T. Ketterl, G. Brauns, A portable discrete frequency NQR explosives detection system. Conference on Detection and Sensing of Mines, Explosive Objects, and Obscured Targets XXIV, Baltimore, MD, 2019.
- [15] P. Hemmani, A.K. Rajarajan, G. Joshi, S.V.G. Ravindranath, Ieee, N-14 NQR spectrometer for explosive detection: A Review, International Conference on Automatic Control and Dynamic Optimization Techniques (ICACDOT), Int Inst Informat Technol, Pune, INDIA, 2016, pp. 1120–1125.
- [16] T.M. Osan, L.M.C. Cerioni, J. Forgue, J.M. Olle, D.J. Pusiol, NQR: From imaging to explosives and drugs detection, *Physica B-Condensed Matter* 389 (1) (2007) 45–50.
- [17] A. Konnai, T. Asaji, H. Nohmi, N. Odano, Development of NQR explosive detection technique for transportation security, *Sci. Technol. Energetic Mater.* 70 (3–4) (2009) 55–61.
- [18] C. Fuche, J. Deseille, Ion mobility spectrometry: a tool to detect narcotics and explosives, *Actual. Chim.* 342–43 (2010) 91–95.
- [19] T.L. Buxton, P.D. Harrington, Trace explosive detection in aqueous samples by solid-phase extraction ion mobility spectrometry (SPE-IMS), *Appl. Spectrosc.* 57 (2) (2003) 223–232.
- [20] L.V. Haley, J.M. Romeskie, Gc-ims., A technology for many applications, in: Conference on Enforcement and Security Technologies, Boston, Ma, 1998, pp. 375–383.
- [21] J.M. Perr, K.G. Furton, J.R. Almirall, Application of a SPME-IMS detection system for explosives detection, Conference on Sensors, and Command, Control, Communications, and Intelligence (C31) Technologies for Homeland Security and Homeland Defense IV, Orlando, FL, 2005, pp. 667–672.
- [22] A. Zalewska, W. Pawlowski, W. Tomaszewski, Limits of detection of explosives as determined with IMS and field asymmetric IMS vapour detectors, *Forensic Sci. Int.* 226 (1–3) (2013) 168–172.

- [23] W. Huang, E. Smarsly, J.S. Han, M. Bender, K. Seehafer, I. Wacker, R.R. Schroder, U.H.F. Bunz, Truxene-based hyperbranched conjugated polymers: fluorescent micelles detect explosives in water, *ACS Appl. Mater. Interfaces* 9 (3) (2017) 3068–3074.
- [24] W.J. Peveler, A. Roldan, N. Hollingsworth, M.J. Porter, I.P. Parkin, Multichannel detection and differentiation of explosives with a quantum dot array, *ACS Nano* 10 (1) (2016) 1139–1146.
- [25] X.H. Wang, Y.Z. Guo, D. Li, H. Chen, R.C. Sun, Fluorescent amphiphilic cellulose nanoaggregates for sensing trace explosives in aqueous solution, *Chem. Commun.* 48 (45) (2012) 5569–5571.
- [26] Y. Salinas, R. Martinez-Manez, M.D. Marcos, F. Sancenon, A.M. Costero, M. Parra, S. Gil, Optical chemosensors and reagents to detect explosives, *Chem. Soc. Rev.* 41 (3) (2012) 1261–1296.
- [27] W.F. Shu, C.W. Guan, W.H. Guo, C.Y. Wang, Y.J. Shen, Conjugated poly (aryleneethynylene)s and their application in detecting explosives, *J. Mater. Chem.* 22 (7) (2012) 3075–3081.
- [28] C.E. Hay, J. Lee, D.S. Silvester, A methodology to detect explosive residues using a gelled ionic liquid based field-deployable electrochemical device, *J. Electroanal. Chem.* 872 (2020).
- [29] B. Ju, Y. Wang, Y.M. Zhang, T. Zhang, Z.H. Lu, M.J. Li, S.X.A. Zhang, Photostable and Low-Toxic Yellow-Green Carbon Dots for Highly Selective Detection of Explosive 2,4,6-Trinitrophenol Based on the Dual Electron Transfer Mechanism, *ACS Appl. Mater. Interfaces* 10 (15) (2018) 13040–13047.
- [30] X.K. Tian, H. Peng, Y. Li, C. Yang, Z.X. Zhou, Y.X. Wang, Highly sensitive and selective paper sensor based on carbon quantum dots for visual detection of TNT residues in groundwater, *Sens. Actuators B* 243 (2017) 1002–1009.
- [31] H.H. Fan, G.Q. Xiang, Y.L. Wang, H. Zhang, K.K. Ning, J.Y. Duan, L.J. He, X. M. Jiang, W.J. Zhao, Manganese-doped carbon quantum dots-based fluorescent probe for selective and sensitive sensing of 2,4,6-trinitrophenol via an inner filtering effect, *Spectrochimica Acta Part a-Molecular and Biomolecular, Spectroscopy* 205 (2018) 221–226.
- [32] F.B. Sen, N. Begic, M. Bener, R. Apak, Fluorescence turn-off sensing of TNT by polyethylenimine capped carbon quantum dots, *Spectrochim. Acta Part a-Mol. Biomol. Spectrosc.* 271 (2022).
- [33] F. Ghasemi, M.R. Hormozi-Nezhad, Determination and identification of nitroaromatic explosives by a double-emitter sensor array, *Talanta* 201 (2019) 230–236.
- [34] M. Yang, J.F. Xu, H.H. Ma, M.Z. Lei, X.J. Ni, Z.W. Shen, B.Y. Zhang, J. Tian, Microstructure development during explosive welding of metal foil: morphologies, mechanical behaviors and mechanisms, *Comp. Part B-Eng.* 212 (2021).
- [35] O. Adegoke, N.N. Daeid, Colorimetric optical nanosensors for trace explosive detection using metal nanoparticles: advances, pitfalls, and future perspective, *Emerg. Topics Life Sci.* 5 (3) (2021) 367–379.
- [36] X.W. Yan, M. Gharib, L. Esrafil, S.J. Wang, K.G. Liu, A. Morsali, Ultrasound irradiation assisted synthesis of luminescent nano amide-functionalized metal-organic frameworks; application toward phenol derivatives sensing, *Front. Chem.* 10 (2022).
- [37] D. Kotsikau, M. Ivanovskaya, Metal oxide semiconductor sensors for detection of toxic and explosive gases, in: *NATO Advanced Research Workshop on Electronic Noses and Sensors for the Detection of Explosives*, Warwick, England, 2003, pp. 93–115.
- [38] Z. Zhao, X.J. Li, G. Tao, C.X. Du, CuCr bulk alloy produced by mechanical alloying and explosive compaction, *Trans. Nonferrous Met. Soc. Chin.* 19 (2009) S626–S629.
- [39] J.H. Lee, S. Kang, J.Y. Lee, J. Jaworski, J.H. Jung, Instant Visual Detection of Picogram Levels of Trinitrotoluene by Using Luminescent Metal-Organic Framework Gel-Coated Filter Paper, *Chemistry-a European Journal* 19 (49) (2013) 16665–16671.
- [40] X.Y. Feng, L.H. Zeng, D.T. Zou, Z.Z. Zhang, G.H. Zhong, S.Y. Peng, L.P. Liu, L. P. Chen, J.Y. Zhang, Trace-doped metal-organic gels with remarkably enhanced luminescence, *RSC Adv.* 7 (59) (2017) 37194–37199.
- [41] C. Wang, L. Tian, W. Zhu, S.Q. Wang, P. Wang, Y. Liang, W.L. Zhang, H.W. Zhao, G. T. Li, Dye@bio-MOF-1 Composite as a Dual-Emitting Platform for Enhanced Detection of a Wide Range of Explosive Molecules, *ACS Appl. Mater. Interfaces* 9 (23) (2017) 20076–20085.
- [42] L. Liu, R. Ding, Y.Y. Mao, B.Q. Sun, Theoretical investigations on the nitro-explosive sensing process of a MOF sensor: Roles of hydrogen bond and pi-pi stacking, *Chem. Phys. Lett.* 793 (2022).
- [43] S.J. Dong, J.S. Hu, K. Wu, M.D. Zheng, A Mg(II)-MOF as recyclable luminescent sensor for detecting TNP with high selectivity and sensitivity, *Inorg. Chem. Commun.* 95 (2018) 111–116.
- [44] L. Yang, Y.L. Liu, C.G. Liu, F. Ye, Y. Fu, A luminescent sensor based on a new Cd-MOF for nitro explosives and organophosphorus pesticides detection, *Inorg. Chem. Commun.* 122 (2020).
- [45] T.T. Wang, Y.Y. Jia, Q. Chen, R. Feng, S.Y. Tian, T.L. Hu, X.H. Bu, A new luminescent metal-organic framework for selective sensing of nitroaromatic explosives, *Science China-Chemistry* 59 (8) (2016) 959–964.
- [46] D. Xincun, W. Guangfa, D. Zhuohua, Recent Progress in Colorimetric/fluorescent Sensing toward Improvised Explosives(Invited), *Acta Photonica Sinica* 51 (8) (2022).
- [47] G.H. Hong, C. Qian, P.C. Xue, X.L. Liu, Q.Q. Wang, M.Y. Liu, P. Gong, R. Lu, Linear Oligocarbazole-Based Organogelators: Synthesis and Fluorescent Probing of Explosives, *Eur. J. Org. Chem.* 2014 (28) (2014) 6155–6162.
- [48] Y.T. Nguyen, S. Shin, K. Kwon, N. Kim, S.W. Bae, BODIPY-based fluorescent sensors for detection of explosives, *J. Chem. Res.* 47 (2) (2023).
- [49] A. Chowdhury, P.S. Mukherjee, Electron-rich triphenylamine-based sensors for picric acid detection, *J. Org. Chem.* 80 (8) (2015) 4064–4075.
- [50] B. Liu, B.Z. Tang, Aggregation-induced emission: more is different, *Angew. Chem. Internat. Ed.* 59 (25) (2020) 9788–9789.
- [51] Y.W. Lu, Y.Q. Tan, Y.Y. Gong, H. Li, W.Z. Yuan, Y.M. Zhang, B.Z. Tang, High efficiency D-A structured luminogen with aggregation-induced emission and mechanochromic characteristics, *Chin. Sci. Bull.* 58 (22) (2013) 2719–2722.
- [52] Y.Q. Dong, J.W.Y. Lam, A.J. Qin, Z. Li, J.X. Sun, H.S. Kwok, B.Z. Tang, Aggregation-induced emission. Conference on Organic Light Emitting Materials and Devices X, San Diego, CA, 2006.
- [53] Y.F. Zuo, R.T.K. Kwok, J.W. Sun, J.W.Y. Lam, B.Z. Tang, Aggregation-induced emission macromolecular materials for antibacterial applications, *Macromol. Rapid Commun.* (2023).
- [54] P.B. Han, H. Xu, Z.F. An, Z.Y. Cai, Z.X. Cai, H. Chao, B. Chen, M. Chen, Y. Chen, Z. G. Chi, S.T. Dai, D. Ding, Y.P. Dong, Z.Y. Gao, W.J. Guan, Z.K. He, J.J. Hu, R. Hu, Y. X. Hu, Q.Y. Huang, M.M. Kang, D.X. Li, J.S. Li, S.Z. Li, W.L. Li, Z. Li, X.L. Lin, H. Y. Liu, P.Y. Liu, X.D. Lou, C. Lu, D.G. Ma, H.L. Ou, J. Ouyang, Q. Peng, J. Qian, A. J. Qin, J.M. Qu, J.B. Shi, Z.G. Shuai, L.H. Sun, R. Tian, W.J. Tian, B. Tong, H. L. Wang, D. Wang, H. Wang, T. Wang, X. Wang, Y.C. Wang, S.Z. Wu, F. Xia, Y. J. Xie, K. Xiong, B. Xu, D.P. Yan, H.B. Yang, Q.Z. Yang, Z.Y. Yang, L.Z. Yuan, W. Z. Yuan, S.Q. Zang, F. Zeng, J.J. Zeng, Z. Zeng, G.Q. Zhang, X.Y. Zhang, X.P. Zhang, Y. Zhang, Y.F. Zhang, Z.J. Zhang, J. Zhao, Z. Zhao, Z.H. Zhao, Z.J. Zhao, B.Z. Tang, Aggregation-induced emission, *Prog. Chem.* 34 (1) (2022) 1–130.
- [55] Z. Sheng, B. Guo, D. Hu, S. Xu, W. Wu, W.H. Liew, K. Yao, J. Jiang, C. Liu, H. Zheng, B. Liu, Bright aggregation-induced-emission dots for targeted synergetic NIR-II fluorescence and NIR-I photoacoustic imaging of orthopedic brain tumors, *Adv. Mater.* (2018) e1800766.
- [56] J. Qi, C. Sun, D. Li, H. Zhang, W. Yu, A. Zebibula, J.W.Y. Lam, W. Xi, L. Zhu, F. Cai, P. Wei, C. Zhu, R.T.K. Kwok, L.L. Streich, R. Prevedel, J. Qian, B.Z. Tang, Aggregation-Induced Emission Luminogen with Near-Infrared-II Excitation and Near-Infrared-I Emission for Ultradeep Intravital Two-Photon Microscopy, *ACS Nano* 12 (8) (2018) 7936–7945.
- [57] M. Hou, Y.C. Liu, W. Zhou, J.D. Zhang, F.D. Yu, Y. Zhang, G.J. Liu, G.W. Xing, Water-soluble AIE-active fluorescent organic nanoparticles: design, preparation and application for specific detection of cyanide in water and food samples, *Chem. Asian J.* 16 (15) (2021) 2014–2017.
- [58] W.M. Wan, D. Tian, Y.N. Jing, X.Y. Zhang, W. Wu, H. Ren, H.L. Bao, NBN-Doped Conjugated Polycyclic Aromatic Hydrocarbons as an AIEgen Class for Extremely Sensitive Detection of Explosives, *Angew. Chem. Int. Ed. Engl.* 57 (47) (2018) 15510–15516.
- [59] F. Neese, Software update: the ORCA program system, version 4.0, *Wiley Interdisciplinary Reviews: Computational Molecular, Science* 8 (1) (2018) e1327.
- [60] H. Kruse, S. Grimme, A geometrical correction for the inter- and intra-molecular basis set superposition error in Hartree-Fock and density functional theory calculations for large systems, *J. Chem. Phys.* 136 (15) (2012) 154101.
- [61] L. Xu, P. Li, Direct introduction of a naphthalene-1, 8-diamino boryl [B (dan)] group by a Pd-catalysed selective boryl transfer reaction, *Chem. Commun.* 51 (26) (2015) 5656–5659.
- [62] C.-Y. Lee, S.-J. Ahn, C.-H. Cheon, Protodeboronation of ortho- and para-phenol boronic acids and application to ortho and meta functionalization of phenols using boronic acids as blocking and directing groups, *J. Org. Chem.* 78 (23) (2013) 12154–12160.
- [63] S. Ding, Q. Ma, M. Zhu, H. Ren, S. Tian, Y. Zhao, Z. Miao, Direct Transformation from Arylamines to Aryl Naphthalene-1, 8-diamino Boronamides: A Metal-Free Sandmeyer-Type Process, *Molecules* 24 (3) (2019) 377.
- [64] C. Cheng, L. Chao-Yi, S.-A. Shahzad, Z. Hui-Peng, Y. Cong, J. Xing, Phenothiazine and BN-doped AIE probes integrated fluorescence sensor array for detection and discrimination of nitro explosives, *Chin. J. Anal. Chem.* 48 (7) (2020) e20075–e20080.
- [65] D. Zhang, F. Xu, Q. Lu, R. Zhang, J. Xia, Poly (3-amino-carbazole) derivatives containing 1, 10-phenanthroline and 8-hydroxyquinoline ligands: Synthesis, properties and application as ion sensors, *Spectrochim. Acta A Mol. Biomol. Spectrosc.* 295 (2023) 122608.
- [66] K. Liu, Z. Hu, A novel conjugated polymer consists of benzimidazole and benzothiadiazole: synthesis, photophysics properties, and sensing properties for Pd²⁺, *J. Polym. Sci.* 58 (6) (2020) 831–842.
- [67] K.C. Gross, P.G. Seybold, Substituent effects on the physical properties and pKa of phenol, *Int. J. Quantum Chem.* 85 (4–5) (2001) 569–579.